Geological Survey
of Canada

Current Research
2001-D17

A diagenetic study of dolostone of the Lower Ordovician Romaine Formation, Anticosti Island, Quebec

G. Chi and D. Lavoie

2001

Natural Resources Canada
Ressources naturelles Canada

Canada

Catalogue No M44-2001/D17E
ISBN 0-660-18442-7

A copy of this publication is also available for reference by depository libraries across Canada through access to the Depository Services Program's website at http://dsp-psd.pwgsc.gc.ca

A free digital download of this publication is available from the Geological Survey of Canada Bookstore web site:

http://gsc.nrcan.gc.ca/bookstore/

Click on Free Download.

Authors' addresses

G. Chi *(guchi@nrcan.gc.ca)*
D. Lavoie *(delavoie@nrcan.gc.ca)*
Quebec Geoscience Centre
2535 Laurier Blvd.
C.P. 7500
Sainte-Foy, Québec
G1V 4C7

A diagenetic study of dolostone of the Lower Ordovician Romaine Formation, Anticosti Island, Quebec[1]

G. Chi and D. Lavoie
GSC Quebec, Québec

Chi, G. and Lavoie, D., 2001: A diagenetic study of dolostone of the Lower Ordovician Romaine Formation, Anticosti Island, Quebec; Geological Survey of Canada, Current Research 2001-D17, 13 p.

Abstract: This study deals with the diagenetic evolution of dolostone of the Romaine Formation, Anticosti Island. Four types of calcite and six types of dolomite were distinguished. According to fluid-inclusion and C-O isotope data, sedimentary micrite, replacement calcite, and early pore-filling calcite were formed in sedimentary and early diagenetic environments. Early replacement dolomite phases were formed in an early burial environment. Later replacement dolomite and pore-filling dolomite as well as minor sphalerite were formed from warm, saline fluids interpreted to be of hydrothermal origin. Significant porosities were produced through dissolution of early replacement dolomite phases by these fluids. Intercrystal porosities were created in later replacement dolomite phases. The dissolution porosities were partly occluded by late-stage calcite, pyrite, and barite. Hydrocarbon inclusions were recorded in late-stage calcite and contemporaneous barite, indicating a hydrocarbon migration event after the porosity-generating processes.

Résumé : La présente étude traite de l'évolution diagénétique de la dolomie de la Formation de Romaine, dans l'île d'Anticosti. Quatre types de calcite et six types de dolomite sont reconnus. D'après les données sur les inclusions fluides et les isotopes de C et O, de la micrite sédimentaire, de la calcite de remplacement et de la calcite de remplissage de porosité précoce se sont formées dans des milieux sédimentaires et de diagenèse précoce. De la dolomite de remplacement précoce s'est formée dans un milieu d'enfouissement précoce. De la dolomite de remplacement plus tardive et de la dolomite de remplissage de porosité ainsi que des quantités mineures de sphalérite se sont formées à partir de fluides salins chauds vraisemblablement d'origine hydrothermale. La dissolution des dolomites de remplacement précoces par ces fluides a produit des porosités importantes. Des porosités intercristallines ont été créées dans des dolomites de remplacement plus tardives. Ces pores de dissolution ont été colmatés en partie par de la calcite tardive, de la pyrite et de la barytine. Des inclusions d'hydrocarbures se rencontrent dans de la calcite tardive et de la barytine contemporaine, indiquant qu'un épisode de migration des hydrocarbures a suivi la porogenèse.

[1] Contribution to the Appalachian Foreland and St. Lawrence Platform NATMAP Project

INTRODUCTION

The Romaine Formation on Anticosti Island consists of Lower Ordovician carbonate units that were deposited at the Laurentia margin prior to the Taconian Orogeny. Coeval carbonate beds along eastern North America, from Newfoundland to Tennessee, represent an important paleoaquifer associated with karstification, dissolution, and dolomitization which hosts a number of Mississippi Valley-type Zn-Pb deposits (Kesler, 1994). The carbonate beds of the St. George Group in western Newfoundland, for example, were extensively dolomitized and host several Mississippi Valley-type deposits (Lane, 1990; Saunders et al., 1992) as well as petroleum reservoirs (Cooper et al., 1997). Lavoie (D. Lavoie, unpub. report to Shell Canada, 1997) noted that some intervals of the Romaine Formation on Anticosti Island are also highly porous and that bleedings of oil have been reported in these rocks. Therefore, from regional consideration and local observations, the Romaine Formation has the potential of forming petroleum reservoirs if other conditions (sources, conduits, and traps) are met. The purpose of the present study is to investigate the diagenetic evolution of the dolostone beds of the Romaine Formation and the origin of the porosities.

A total of 24 samples of the Romaine Formation were selected from three drill cores (NACP, LGCP, LGPL) on Anticosti Island and from a quarry (QFT) north of Mingan Islands (Fig. 1). These samples are a subset of those studied by Lavoie (D. Lavoie, unpub. report to Shell Canada, 1997). The criteria for selecting samples are described as follows. First, since high porosities are developed mainly in dolostone, we selected 22 dolostone samples versus 2 limestone samples, the latter being mainly for purpose of reference. Second, because not all dolostone beds are porous, we selected 16 porous versus 6 nonporous dolostone samples in order to identify which dolomite phases are associated with porosity generation. Third, it was noticed that some samples contain fractures that are partly or completely filled with dolomite, calcite, and sulphides, whereas other samples are more or less homogeneous. We selected 7 fractured versus 17 nonfractured samples in order to investigate the role of fracturing in porosity generation. The general information about each sample (location, rock type, porosity, etc.) is listed in Table 1.

This study includes three aspects: 1) petrography, 2) fluid-inclusion microthermometry, and 3) C-O isotopes of carbonate and S isotopes of sulphides and sulphate. The petrographic study aims to identify different mineral phases, their paragenesis, and their relationships to porosities. Fluid-inclusion microthermometry is used to estimate the formation temperatures of a specific mineral phase, and the salinities of the fluids that were involved. Carbon and oxygen isotope data are used in conjunction with fluid-inclusion data to further evaluate the composition and thermal conditions of the parent fluids. Finally, S isotopes of fracture-filling sulphides and sulphate are used to evaluate the sources of sulphur and the possible roles of sulphide precipitation on porosity generation.

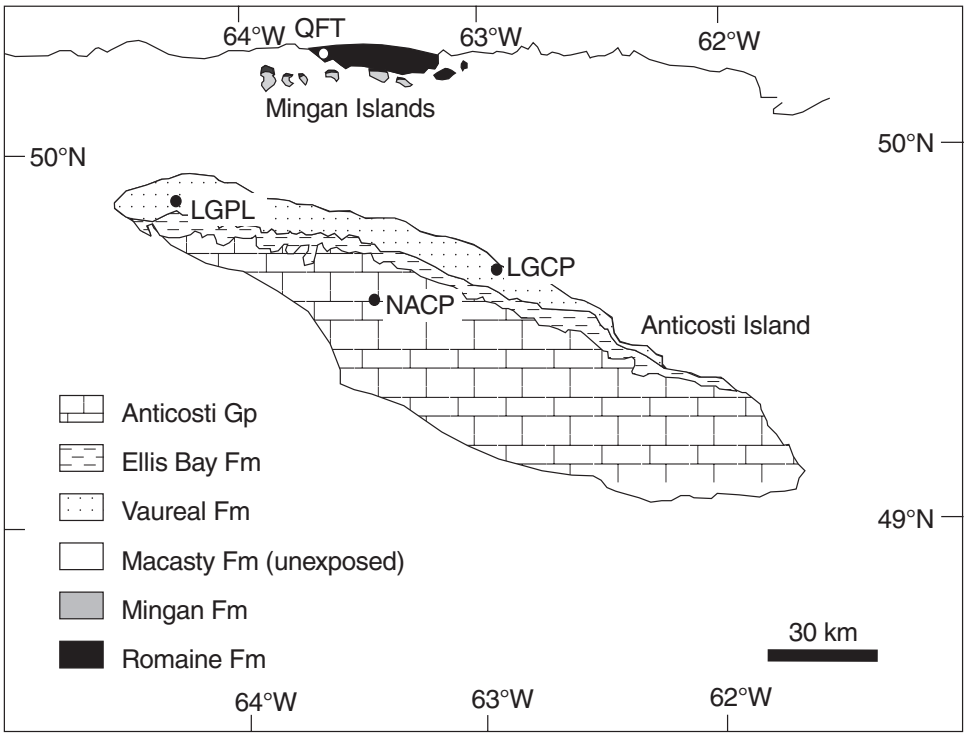

Figure 1. *General geology of Anticosti Island and location of drill wells from which samples of this study were collected (after Lavoie, 1997).*

Table 1. List of samples from the Romaine Formation, Anticosti Island.

Core	Sample#	Depth (m)	Rock type	Porosity	Fractures
NACP	NACP-13	1614.22	Dolostone	~0%	No
	NACP-24	1650.95	Dolostone	~0%	No
	NACP-40	1704.29	Dolostone	~10%	No
	NACP-54	1758.64	Dolostone	~1%	No
	NACP-38	1701.39	Dolostone	~15%	No
	NACP-39	1702.92	Dolostone	~10%	No
	NACP-46	1733.09	Dolostone	~15%	No
	NACP-44	1729.48	Dolostone	~2%	Yes
	NACP-51	1748.10	Dolostone	~5%	Yes
	NACP-37	1700.40	Dolostone	~2%	Yes
	NACP-35	1697.40	Dolostone	~0%	Yes
LGCP	LGCP-33	711.17	Limestone	~0%	No
	LGCP-31	752.36	Limestone	~0%	Yes
	LGCP-3	937.87	Dolostone	~0%	No
	LGCP-4	937.44	Dolostone	~0%	No
	LGCP-14	865.63	Dolostone	~10%	No
	LGCP-18	822.90	Dolostone	~20%	No
	LGCP-25	785.37	Dolostone	~5%	No
	LGCP-26	782.36	Dolostone	~10%	No
	LGCP-24	788.11	Dolostone	~10%	Yes
	LGCP-28	772.24	Dolostone	~3%	Yes
LGPL	LGPL-3	1380.00	Dolostone	~0%	No
	LGPL-10	1593.80	Dolostone	~7%	No
QFT quarry	QFT-1		Dolostone	~7%	No

GEOLOGICAL SETTING

Anticosti Island is part of the St. Lawrence platform that covered the southeastern edge of the Canadian Shield in the Paleozoic. The strata of the St. Lawrence platform range from late Proterozoic to Devonian, recording geological evolution from rifting (late Proterozoic), through passive margin (Cambrian to Early Ordovician), to foreland basin (Middle Ordovician and later) (Sanford, 1993).

The strata in the Anticosti Island area consist of, in ascending order, the Romaine, Mingan, Macasty, Vaureal, and Ellis Bay formations and the Anticosti Group, ranging from Early Ordovician to Early Silurian. The Romaine Formation, consisting of mainly dolostone, was formed in the passive-margin stage in the Early Ordovician. It is exposed on Mingan Islands (to the north of Anticosti Island; Fig. 1) and encountered by drills in Anticosti Island. On Mingan Islands, the top of the Romaine Formation is cut by an unconformity (the regional Sauk–Tippecanoe sequence boundary of Knight et al. (1991)) and associated paleokarst features (Desrochers, 1985; Desrochers and James, 1988), which is overlain by basal sandstone and overlying carbonate of the Mingan Formation. The Mingan Formation is overlain by clastic rocks of the Middle to Late Ordovician Macasty Formation, which show good hydrocarbon source-rock potential (Bertrand, 1991). The Late Ordovician Vaureal Formation consists of clastic rocks in the lower part and carbonate in the upper part, followed by carbonate of the Late Ordovician Ellis Bay Formation and the Early Silurian Anticosti Group.

The strata in the Anticosti Island area are not folded, but dip slightly to the south-southwest. A number of synsedimentary normal faults, striking east-northeast to west-northwest, have been postulated by facies distribution (D. Lavoie, unpub. report to Shell Canada, 1997) and indicated by seismic data. Some of these faults may have experienced reactivation, in relation to tectonic events in the Appalachian Mountains.

PETROGRAPHY

A detailed petrographic study of the selected samples was carried out using the following methods: visual examination of hand specimen, Dickson staining of polished slabs, conventional microscopy (transmitted and reflected light), and cathodoluminoscopy of polished thin sections. Six types of dolomite and four types of calcite were distinguished based on their crystal shapes and sizes, Dickson staining, cathodoluminescence, and relationships to porosity (Table 2). The proportions of each carbonate phase as well as other minerals are listed in Table 3. The two limestone samples (LGCP-33, LGCP-31) consist of only calcite and minor pyrite, whereas the dolostone samples consist of mainly dolomite with variable amounts of other minerals, among which the more frequently observed are pyrite, detrital quartz and feldspar, and barite (Table 3). Minor amounts of sphalerite occur in four dolostone samples (NACP-54, NACP-51,

Table 2. Types of dolomite and calcite and their petrographic features.

Type	Shape	Size (mm)	Dickson staining	Cathodoluminescence	Relation to porosity
Dolomite					
RD1	Anhedral to subhedral, mainly nonplanar	0.005–0.03	Blue to light blue	Dull reddish orange	Prior to dissolution porosity
RD2	Anhedral to euhedral, nonplanar to planar	0.02–0.12	Very light blue to none	Dull reddish orange	Prior to dissolution porosity
RD3	Anhedral to euhedral, planar to nonplanar	0.02–0.5	Non to light blue, with or without a blue rim	Dull reddish orange with or without a bright reddish orange rim	Abundant intercrystal porosity
RD4	Anhedral to euhedral, planar to nonplanar	0.02–0.12	Blue to light blue	Dull reddish orange	Abundant intercrystal porosity
PD1	Subhedral to euhedral, planar to saddle	0.1–0.5	None	Very dull reddish orange	Partly fill or coat dissolution porosity
PD2	Subhedral to euhedral, planar to saddle	0.1–3	Light blue to blue	Dull reddish orange with or without a bright reddish orange rim	Partly fill or coat dissolution porosity
Calcite					
SC	Anhedral	A few micrometres	Red	Yellow	None
RC	Anhedral	0.005–0.3	Red	Dull	None
PC1	Anhedral	0.1–0.5	Red	Yellow/dull zoned	Filling pores
PC2	Anhedral	0.05–6	Red to purple	Yellowish orange with or without dull patches or irregular zones	Filling pores or fractures

RD = replacement dolomite; PD = pore-filling dolomite; SC = sedimentary calcite; RC=replacement calcite; PC=pore-filling calcite.

Table 3. Mineral components (%) of samples from the Romaine Formation, Anticosti Island.

Sample#	RD1	RD2	RD3	RD4	PD1	PD2	SC	RC	PC1	PC2	Det.	Aut. Qz	Pyrite	Sphalerite	Barite	Gypsum	Halite
NACP-13	40	57									2		1				
NACP-24	78	20								1	1		t				
NACP-40	9		80		1					10		t	t		t		
NACP-54	60	20			10					9		t	t	1			
NACP-38		82			5					10	1		1		1		
NACP-39		85	12	2						1	t				t		
NACP-46			99										t		1		
NACP-44 (host)			85							14			1		t		
NACP-44 (vein)										75					25		
NACP-51 (host)		15	83			2									t		
NACP-51 (vein1)						35				20			39	5	1		
NACP-51 (vein2)										5			40		55		
NACP-37	25	45				5				5			19		1		
NACP-35	80	15								2	1		1	1			
LGCP-33							70	28	1				1				
LGCP-31 (host)							70	25	5								
LGCP-31 (vein)										70			30				
LGCP-4	7	90								1	1		1				
LGCP-3		60			25			10		15	t		t				
LGCP-14		70	30														
LGCP-18		24	75								t		1				
LGCP-25	50	45			5						t		t	t			
LGCP-26		35		65									t				
LGCP-24		73	10			10				2			5		t		
LGCP-28 (host)	20	75				2				2	1						
LGCP-28 (vein)										40			60				
LGPL-3	40	55				5					t				t	t	t
LGPL-10		30	53			10				2		t	1		4		
QFT-1		80	20										t				

Abbreviations: RD = replacement dolomite; PD = pore-filling dolomite; SC = sedimentary calcite; RC = replacement calcite; PC = pore-filling calcite; Det. = detrital quartz and feldspar; Aut. Qz = authigenic quartz; t = trace.

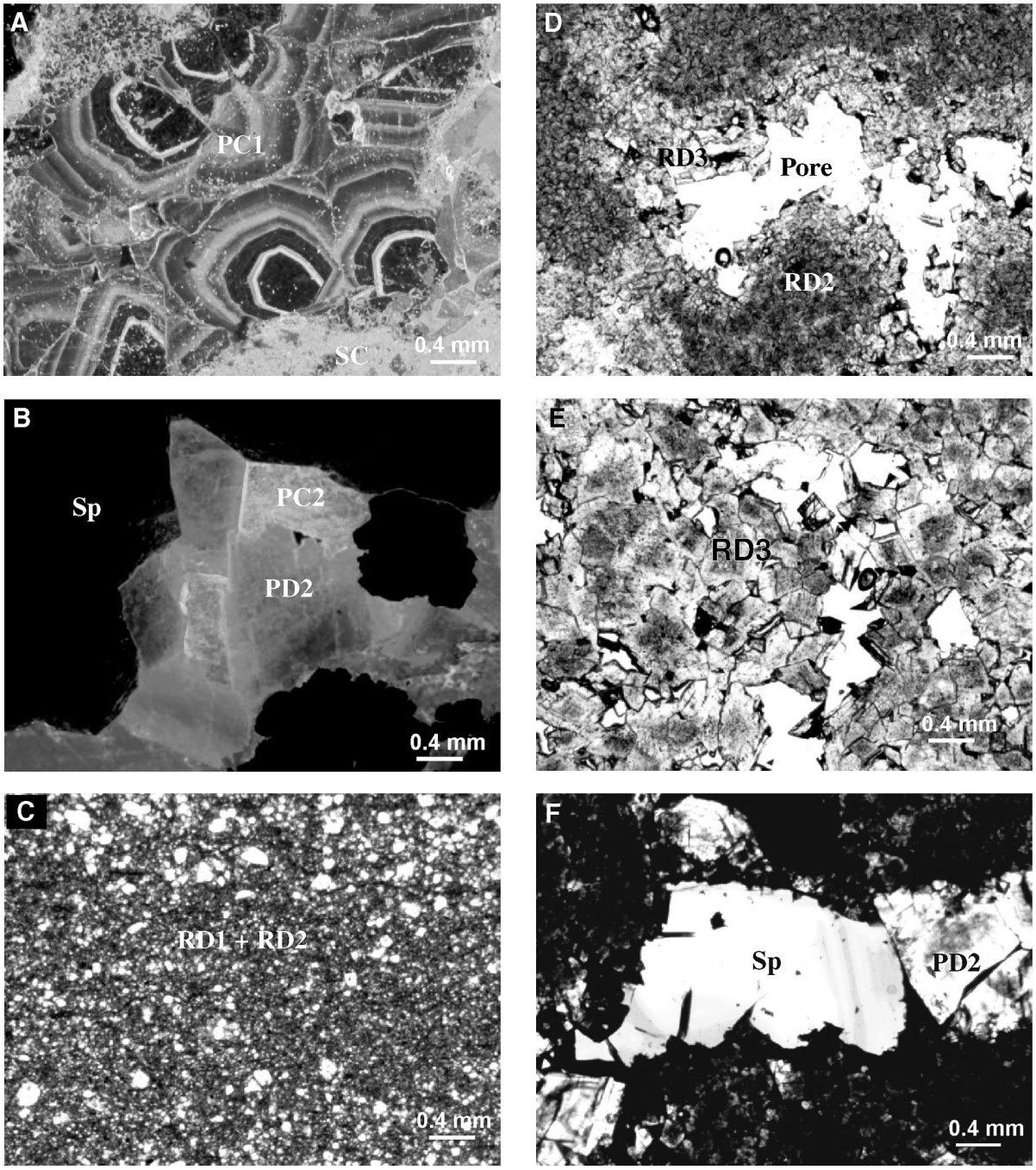

Figure 2. *Photomicrographs showing various diagenetic minerals and features of dolostone samples of the Romaine Formation.* ***A)*** *Early pore-filling calcite (PC1) is characterized by zoned yellow to dull cathodoluminescence; SC = sedimentary calcite.* ***B)*** *Pore-filling dolomite (PD2) and late pore-filling calcite (PC2) show dull reddish-orange and yellowish orange cathodoluminescence; Sp = sphalerite.* ***C)*** *Early replacement dolomite (first- and second-phase dolomite: RD1 and RD2) preserve beddings. Transmitted light.* ***D)*** *Dissolution porosity. Third-phase replacement dolomite (RD3) forms a halo around the dissolution pores. Transmitted light.* ***E)*** *Intercrystal porosity associated with third-phase replacement dolomite (RD3).* ***F)*** *Sphalerite (Sp) associated with pore-filling dolomite (PD2).*

NACP-35, LGCP-25), and trace amounts of authigenic quartz, gypsum, and halite were observed in some samples (Table 3).

Sedimentary micrite (sedimentary calcite) is very fine grained, yellow luminescent, Fe-poor (Dickson staining = red), and has no visible porosity. Replacement calcite is anhedral, replacing micrite or fossils, 0.005–0.3 mm, Fe-poor, and dull luminescent. Sedimentary and replacement calcite are the major components of the limestone samples. An early phase of pore-filling calcite is anhedral, 0.1–0.5 mm, Fe-poor, and is characterized by well zoned yellow/dull luminescence (Fig. 2A). A late phase of pore-filling calcite is anhedral, 0.05–6 mm, Fe-poor to Fe-rich, fills fractures or residual pores left by dolomitization, and shows yellowish-orange luminescence with or without patches or irregular zones of dull luminescence (Fig. 2B).

The first phase of replacement dolomite is anhedral to subhedral, mainly nonplanar, very fine grained (0.005–0.03 mm), Fe-rich (Dickson staining = blue to light blue), and shows dull reddish-orange luminescence. The second phase of replacement dolomite is similar to the first phase except that it is coarser (0.02–0.12 mm) and contains less Fe. The first and sceond phases can form parallel bands, preserving sedimentary bedding (Fig. 2C). These two phases of dolomite are the major components of the dolostone samples (*see* Table 3). They do not possess intercrystal porosities, but are subject to later dissolution that produces pore space (Fig. 2D). The third phase of replacement dolomite is anhedral to euhedral, planar to nonplanar, 0.02–0.5 mm, Fe-poor with or without a Fe-rich rim, dull reddish-orange luminescent with or without a bright reddish-orange rim. The fourth phase of replacement dolomite is similar to the third phase except that it is Fe-rich. Both third and fourth phase replacement dolomite have abundant intercrystal porosities (Fig. 2E), and may form a halo around dissolution pores (Fig. 2D), indicating that they are related to the processes that dissolve the first and second phase replacement dolomite. The brightly luminescent rim of third-phase crystals are sometimes discontinuous, suggesting extended dissolution after the formation of third-phase replacement. Two types of pore-filling dolomite are distinguished. The first phase is subhedral to euhedral, planar to saddle, 0.1–0.5 mm, Fe-poor, very dull reddish-orange luminescent, and partly fills or coats dissolution pores. The second phase is similar to the first except that it is Fe-rich and may have a bright reddish-orange luminescent rim (Fig. 2B). The second phase of pore-filling dolomite may fill fractures in addition to dissolution pores.

Sphalerite occurs as anhedral, coarse, yellow to brown crystals filling fractures or dissolution pores in association with first- and second-phase pore-filling dolomite (Fig. 2F). Pyrite occurs either as fine crystals disseminated in replacement dolomite or as coarse crystals coating fractures and pores. Barite fills fractures or residual pores left by first- and second-phase pore-filling dolomite, sphalerite, and pyrite, and is associated with second-phase pore-filling calcite.

The paragenetic sequence is summarized in Figure 3. Sedimentary calcite is followed by replacement calcite, which in turn is succeeded by early pore-filling calcite. These three calcite phases are mainly found in limestones that have not been subject to dolomitization, and are interpreted to have formed in sedimentary to early diagenetic environments. Because they are inseparable by conventional microdrilling, and possibly have been formed in similar environments, sedimetnary calcite, replacement calcite, and early pore-filling calcite are grouped together (C1, Fig. 3) in the analysis of stable isotopes. The first two phases of replacement dolomite are closely associated with each other, and appear to have been controlled by sedimentary textures, as indicated by bedding-parallel distribution of the two phases. They apparently postdate the three calcite phases, predate other minerals, and were probably formed relatively early in the diagenetic history. Because they are inseparable by microdrilling in some samples, and possibly have been formed in similar environments, the first- and second-phase replacement dolomite are grouped together (D1, Fig. 3) for the convenience of stable isotope study; however, some replacement dolomite that is classified as second phase may have been formed later, and may have overlapped with successive dolomite phases in time. The next two phases of replacement dolomite, apparently postdate first- and second-phase replacement dolomite, and are associated with a dissolution event that created porosities in dolostone composed of the two first phases. In many cases, third-phase replacement dolomite shows a transitional relationship with second-phase replacement dolomite, the main difference being that the third phase has more intercrystal porosities. Because the third- and fourth-phase replacement dolomite types are similar in paragenetic position and because fourth-phase replacement dolomite is restricted in only two

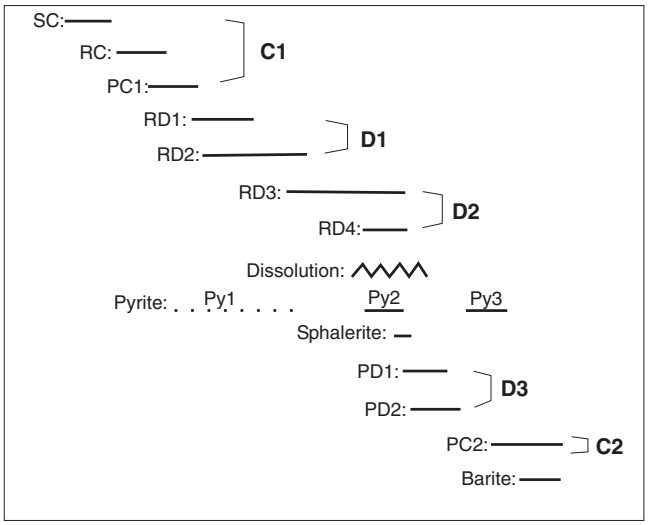

Figure 3. *Generalized paragenetic sequence of the dolostone of the Romaine Formation. SC = sedimentary calcite, RC = replacement calcite, PC1 = early pore-filling calcite, RD1 = first-phase replacement dolomite, RD2 = second-phase replacement dolomite, RD3 = third-phase replacement dolomite, RD4 = fourth-phase replacement dolomite, Py = pyrite phases (Py1, Py2, Py3), PD1 = first-phase pore-filling dolomite, PD2 = second-phase pore-filling dolomite, PC2 = late pore-filling calcite.*

samples, they are grouped together (D2, Fig. 3) for the convenience of discussion. Pyrite appears to have been formed in many different stages. Pyrite disseminated in limestone and dolostone and associated with the three calcite phases and the two early replacement dolomite phases were probably formed in early diagenesis (Py1, Fig. 3). A second phase of pyrite (Py2, Fig. 3) is associated with third- and fourth-phase replacement dolomite, or coats dissolution pores and fractures that are filled by sphalerite and first- and second-phase pore-filling dolomite. A third phase of pyrite (Py3, Fig. 3) coats pores or fractures and is succeeded by or co-precipitated with late pore-filling calcite. Sphalerite postdates (partly overlaps) the second phase of pyrite, and predates (partly overlaps?) first- and second-pahse pore-filling dolomite. The two pore-filling dolomite phases do not coexist in the same pores or fractures, but are similar in paragenetic position, and are thus grouped together. They apparently postdate (but possibly overlap) the dissolution event, and may partly overlap with third- and forth-phase replacement dolomite in time. Late pore-filling calcite and barite are similar in paragenetic position; they all postdate the dissolution event as well as first- and second-phase pore-filling dolomite. Late pore-filling calcite is the last carbonate phase observed in our samples, and is responsible for a significant part of occlusion of porosities that were previously created by dissolution or fracturing.

FLUID INCLUSIONS

Doubly polished sections of 16 samples were prepared for fluid-inclusion microthermometry. Fluid inclusions were studied in early pore-filling calcite; second-, third-, and fourth-phase replacement dolomite; first- and second-phase pore-filling dolomite; late pore-filling calcite; and barite. Fluid inclusions occurring as isolated inclusions, in clusters, or randomly distributed in three dimensions are considered as primary or pseudosecondary inclusions (Roedder, 1984). Some of the occurrences of fluid inclusions are shown in Figure 4. The microthermometric results (homogenization temperature and salinity) are shown in Table 4 and Figure 5.

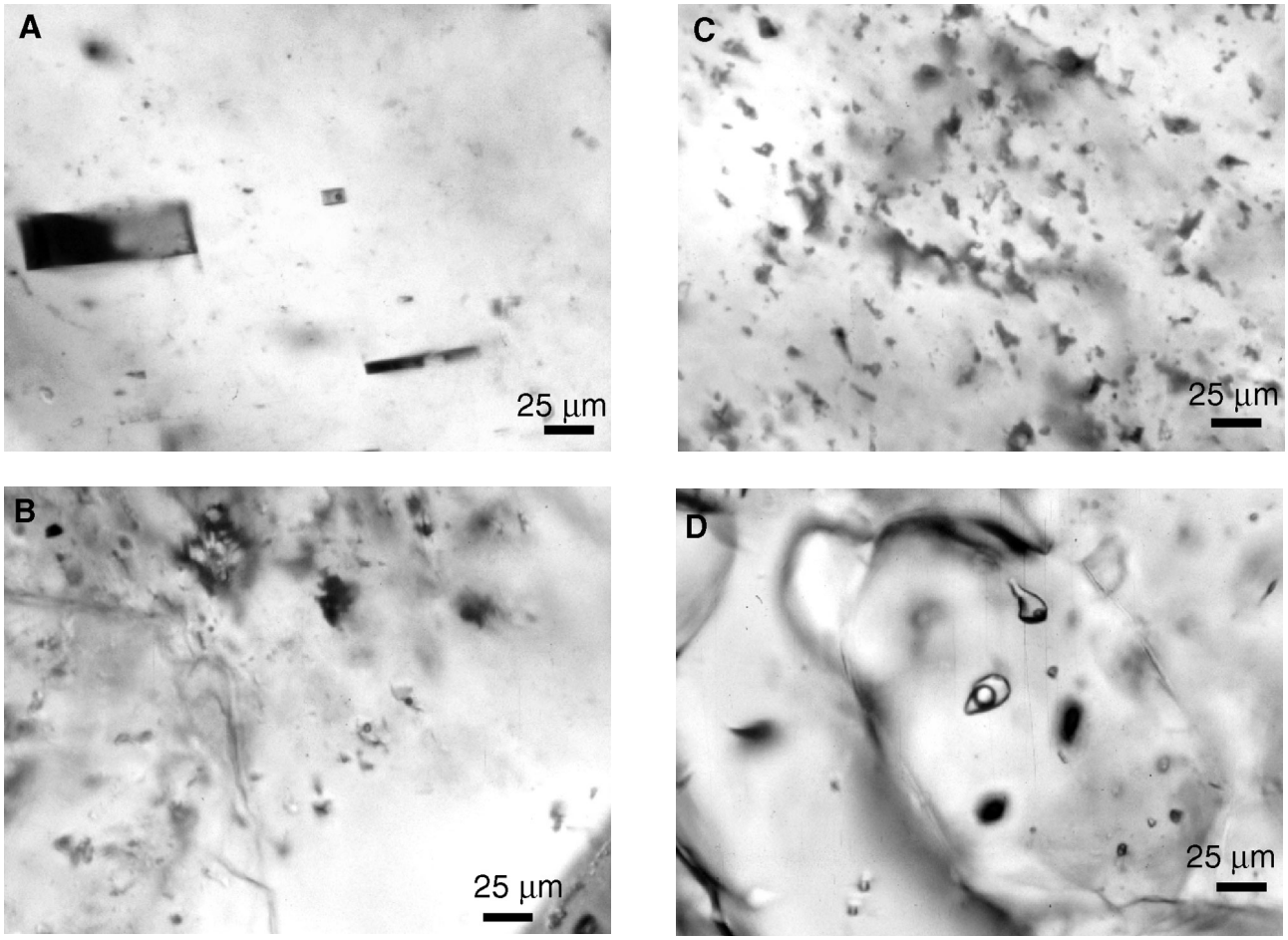

Figure 4. *Photomicrographs showing various occurrences of fluid inclusions.* ***A)*** *An isolated fluid inclusion in third-phase replacement dolomite (RD3).* ***B)*** *Fluid inclusions distributed along the edge of a cloudy core of third-phase replacement dolomite (RD3).* ***C)*** *Randomly distributed fluid inclusions in third-phase replacement dolomite (RD3).* ***D)*** *Oil inclusions in barite.*

Homogenization temperatures (T_h) of fluid inclusions from each mineral phase show wide ranges (*see* Table 4, Fig. 5); however, variations within individual inclusion group (e.g. a cluster) are much smaller, usually less than 15°C, suggesting that post-trapping effects (e.g. stretching) are not important for most of the inclusions studied (Goldstein and Reynolds, 1994). Therefore, the overall ranges of T_h values are believed to reflect the real variation of temperature during the precipitation of each mineral phase. Fluid inclusions from early pore-filling calcite show very low T_h values (59°C). Fluid inclusions from second-phase replacement dolomite have slightly higher T_h values, ranging from 60.3°C to 95.9°C. Fluid inclusions from third-phase replacement dolomite, and first- and second-phase pore-filling dolomite show higher T_h values, ranging from 61.5°C to 131.3°C, 82.9°C to 113.3°C, and 101.4°C to 137.1°C, respectively. Homogenization temperature values of fluid inclusions from late pore-filling calcite and barite are relatively low, ranging from

Table 4. Fluid-inclusion microthermometric data of samples from the Romaine Formation.

Sample	Host mineral	Occurrence	Size (μm)	$T_{m\text{-}ice}$ (°C)		Salinity (wt.% NaCl equiv.)		T_h (°C)	
				Range	Mean (n)	Range	Mean (n)	Range	Mean (n)
NACP-40	RD3	Randomly distributed	7–10	-	-	-	-	112.4–116.8	114.6 (2)
		Randomly distributed	4–6	-20.8	-20.8 (1)	22.9	22.9 (1)	86.9–103.2	93.4 (3)
		Randomly distributed	12	-13.6	-13.6 (1)	17.5	17.5 (1)	116.5	116.5 (1)
		Randomly distributed	6–9	-23.8	-23.8 (1)	23.8	23.8 (1)	71.3–75.1	73.2 (2)
	PC2	Isolated	12	-26.3	-26.3 (1)	24.4	24.4 (1)	72.2	72.2 (1)
		Cluster	7	-	-	-	-	60.3	60.3 (1)
		Cluster	8	-36.2	-36.2 (1)	27.4	27.4 (1)	all-liquid	all-liquid
	Barite	Scattered	8–18	-20.1 to -20.4	-20.2 (3)	22.4–22.6	22.5 (3)	57.4–110.5	83.0 (6)
NACP-38	PD1	Randomly distributed	7	-14.4	-14.4 (1)	18.1	18.1 (1)	82.9	82.9 (1)
		Randomly distributed	5	-	-	-	-	105.1	105.1 (1)
		Randomly distributed	5	-23.6	-23.6 (1)	23.7	23.7 (1)	102.3	102.3 (1)
		Randomly distributed	6–10	-	-	-	-	90.7–102.1	96.4 (2)
	PC2	Cluster	7–13	-32.8	-32.8 (1)	26.5	26.5 (1)	86.4–114.9	104.5 (3)
			6–12	Oil:				65.3–80.5	72.8 (3)
		Isolated	12	-35.0	-35.0 (1)	27.1	27.1 (1)	113.6	113.6 (1)
		Cluster	8–18	-20.2 to -21.8	-21.1 (3)	22.5–23.3	23.0 (3)	60.7–79.3	68.8 (7)
		Isolated	9	-12.0	-12.0 (1)	16.0	16.0 (1)	119.6	119.6 (1)
		Isolated	12	-13.4	-13.4 (1)	17.3	17.3 (1)	98.8	98.8 (1)
		Isolated	15	-36.4	-36.4 (1)	27.4	27.4 (1)	120.8	120.8 (1)
	Barite	Scattered	8–11	-22.2 to -28.9	-25.6 (2)	23.4–25.2	24.3 (2)	68.1–69.8	69.0 (2)
		Scattered	9–10	-16.5 to -17.5	-17.0 (2)	19.8–20.6	20.2 (2)	104.1–110.6	106.6 (3)
NACP-39	RD3	Randomly distributed	5–7	-19.3 to -20.6	-20.0 (2)	21.9–22.8	22.4 (2)	99.8–129.8	114.6 (3)
		Randomly distributed	5	-	-	-	-	102.2	102.2 (1)
		Randomly distributed	5–6	-8.3 to -10.4	-9.4 (2)	12.1–14.4	13.3 (2)	104.1–111.5	107.0 (3)
NACP-46	RD3	Randomly distributed	4–9	-10.5	-10.5 (1)	14.5	14.5 (1)	97.5–109.3	102.0 (4)
		Randomly distributed	5–8	-	-	-	-	86.5–102.6	94.6 (2)
		Isolated	9	-18.6	-18.6 (1)	21.4	21.4 (1)	117.6	117.6 (1)
		Randomly distributed	4–10	-12.1 to -18.5	-15.5 (3)	16.1–21.3	18.9 (3)	92.0–110.6	103.0 (5)
		Randomly distributed	5–9	-20.5	-20.5 (1)	22.7	22.7 (1)	109.5–116.8	112.9 (3)
NACP-44	RD3	Randomly distributed	6–7	-22.4	-22.4 (1)	23.5	23.5 (1)	92.6–113.3	104.8 (3)
		Randomly distributed	6–7	-20.4	-20.4 (1)	22.6	22.6 (1)	83.6–102.0	92.8 (2)
	PC2	Scattered	7–15	-20.2 to -21.6	-20.9 (2)	22.5–23.3	22.9 (2)	88.6–101.7	97.0 (4)
			6–8	Oil:				75.4–82.7	79.1 (2)
		Isolated	9	-29.0	-29.0 (1)	25.2	25.2 (1)	63.9	63.9 (1)
		Isolated	11	-25.2	-25.2 (1)	24.1	24.1 (1)	77.4	77.4 (1)
	Barite	Cluster	8–20	-19.8 to -19.9	-19.9 (2)	22.2–22.3	22.3 (2)	65.7–86.8	75.6 (6)
		Cluster	7–11	-19.9 to -22.8	-21.4 (2)	22.3–22.5	22.4 (2)	60.8–96.1	76.2 (4)
		Scattered	9–12	-20.3 to -22.8	-21.6 (2)	22.6–23.5	23.1 (2)	92.8–100.9	96.9 (2)
			4–12	Oil:				34.3–86.0	58.9 (4)
NACP-51	RD3	Randomly distributed	6–9	-21.3 to -22.4	-21.9 (2)	23.2–23.5	23.4 (2)	96.1–109.2	104.3 (3)
		Randomly distributed	5	-29.8	-29.8 (1)	25.5	25.5 (1)	103.5	103.5 (1)
		Randomly distributed	4–5	-17.2	-17.2 (1)	20.4	20.4 (1)	78.8–101.7	93.3 (3)
		Randomly distributed	9	-21.7	-21.7 (1)	23.3	23.3 (1)	112.0	112.0 (1)
		Randomly distributed	6	-	-	-	-	93.3	93.3 (1)
	PD2	Randomly distributed	5–9	-27.7	-27.7 (1)	24.8	24.8 (1)	99.2–103.6	101.4 (2)

43.4°C to 120.8°C, and 59.9°C to 106.6°C, respectively. Salinity values, which are calculated from last ice-melting temperatures, are also variable. Salinity ranges are similar between different mineral phases, mainly between 15 and 27 wt.% NaCl equivalent (Table 4), which is typical of basinal brines. The variation in salinity within each mineral phase possibly indicates involvement of more than one fluid.

Oil inclusions were observed in late pore-filling calcite and barite in a few samples (NACP-38, NACP-44, LGCP-31). They are mainly colourless under transmitted light (Fig. 4D), fluoresce greenish white under blue light excitation, and always homogenize to liquid phase. Homogenization temperatures of the oil inclusions are lower than those of aqueous inclusions in the same mineral phase (Table 4).

Table 4. (cont.)

Sample	Host mineral	Occurrence	Size (μm)	$T_{m\text{-}ice}$ (°C)		Salinity (wt.% NaCl equiv.)		T_h (°C)	
				Range	Mean (n)	Range	Mean (n)	Range	Mean (n)
		Randomly distributed	7	-18.9	-18.9 (1)	21.6	21.6 (1)	130.3	130.3 (1)
		Cluster	5–9	-16.1	-16.1 (1)	19.5	19.5 (1)	124.4–138.4	131.4 (2)
		Cluster	9–10	-18.7	-18.7 (1)	21.4	21.4 (1)	124.8–129.9	127.4 (2)
		Cluster	9–15	-20.2	-20.2 (1)	22.5	22.5 (1)	119.0–122.1	120.1 (3)
		Cluster	7–10	-25.2	-25.2 (1)	24.1	24.1 (1)	115.8–122.1	118.1 (3)
	PC2	Scattered	6–18	-17.2 to -23.6	-21.4 (2)	20.4–23.7	22.6 (3)	60.0–100.2	77.7 (8)
	Barite	Scattered	8–18	-27.4 to -31.8	-29.2 (4)	24.7–26.2	25.3 (4)	51.5–70.8	59.9 (5)
LGCP-3	PD1	Randomly distributed	6–8	-23.4	-23.4 (1)	23.7	23.7 (1)	85.1–100.1	91.0 (4)
		Randomly distributed	7	-13.6	-13.6 (1)	17.5	17.5 (1)	113.3	113.3 (1)
		Randomly distributed	10–15	-18.8	-18.8 (1)	21.5	21.5 (1)	86.2–111.4	99.6 (3)
	PC2	Cluster	6–7	-	-	-	-	78.3–88.2	83.3 (2)
		Cluster	5–7	-18.0	-18.0 (1)	20.9	20.9 (1)	87.5–93.2	89.8 (3)
LGCP-14	RD2	Randomly distributed	6	-	-	-	-	60.3	60.3 (1)
		Randomly distributed	6–8	-25.5	-25.5 (1)	24.2	24.2 (1)	74.8–92.7	83.8 (2)
	RD3	Isolated	12	-31.2	-31.2 (1)	26.0	26.0 (1)	105.6	105.6 (1)
		Isolated	7	-32.1	-32.1 (1)	26.2	26.2 (1)	97.8	97.8 (1)
		Isolated	14	-21.6	-21.6 (1)	23.3	23.3 (1)	131.3	131.3 (1)
		Isolated	11	-22.0	-22.0 (1)	23.4	23.4 (1)	116.4	116.4 (1)
		Randomly distributed	6–7	-28.6	-28.6 (1)	25.1	25.1 (1)	108.8–118.1	113.5 (2)
		Randomly distributed	6–7	-33.1	-33.1 (1)	26.5	26.5 (1)	98.9–109.5	104.2 (3)
LGCP-18	RD3	Randomly distributed	6–7	-19.2	-19.2 (1)	21.8	21.8 (1)	102.3–104.0	103.2 (2)
		Randomly distributed	6	-26.8	-26.8 (1)	24.6	24.6 (1)	101.3	101.3 (1)
LGCP-28	PC2	Scattered	8–23	-21.9 to -23.0	-22.5 (2)	23.3–23.6	23.5 (2)	59.8–79.3	69.7 (4)
LGCP-31	PC1	Randomly distributed	6–25	-10.8 to -15.6	-13.1 (3)	14.8–19.1	16.9 (3)	34.8–77.4	59.0 (10)
	PC2	Randomly distributed	10–18	-23.4 to -23.5	-23.5 (2)	23.7–23.7	23.7 (2)	33.8–65.7	43.4 (4)
LGPL-10	RD3	Isolated	10	-	-	-	-	82.1	82.1 (1)
		Isolated	7	-	-	-	-	111..3	111.3 (1)
		Isolated	12	-24.2	-24.2 (1)	23.9	23.9 (1)	75.6	75.6 (1)
	PD2	Randomly distributed	5–7	-	-	-	-	96.3–106.3	102.3 (3)
		Randomly distributed	6–8	-23.6	-23.6 (1)	23.7	23.7 (1)	129.3–132.4	130.9 (2)
		Isolated	6	-	-	-	-	137.1	137.1 (1)
		Randomly distributed	5–6	-22.9 to -23.8	-23.4 (2)	23.6–23.8	23.7 (2)	104.6–123.6	114.0 (4)
		Randomly distributed	6–8	-27.3	-27.3 (1)	24.7	24.7 (1)	120.4–136.9	128.4 (3)
QFT-1	RD2	Randomly distributed	5–12	-19.5 to -21.2	-20.4 (2)	22.0–23.2	22.6 (2)	63.8–78.2	70.4 (6)
		Randomly distributed	7–11	-22.3	-22.3 (1)	23.4	23.4 (1)	93.7–98.2	95.9 (3)
		Randomly distributed	6–8	-17.3	-17.3 (1)	20.4	20.4 (1)	55.6–66.6	62.0 (3)
	RD3	Randomly distributed	6–8	-	-	-	-	109.4–114.7	112.1 (2)
		Randomly distributed	8–9	-	-	-	-	71.4–75.0	73.2 (2)
		Cloudy core edge	6–12	-24.3 to -24.6	-24.5 (2)	23.9–24.0	24.0 (2)	95.2–101.8	98.1 (3)
		Cloudy core edge	10–13	-23.6	-23.6 (1)	23.7	23.7 (1)	93.6–97.1	95.4 (2)
		Cloudy core	6–10	-26.3 to -26.8	-26.6 (2)	24.4–24.6	24.5 (2)	61.4–71.6	66.5 (2)
		Isolated	8	-29.2	-29.2 (1)	25.3	25.3 (1)	111.2	111.2 (1)
		Cloudy core	7–9	-21.2	-21.2 (1)	23.2	23.2 (1)	59.4–63.5	61.5 (2)
		Cloudy core	21	-19.3	-19.3 (1)	21.9	21.9 (1)	94.8	94.8 (1)
		Cluster	6–10	-24.0 to -25.2	-24.6 (2)	23.8–24.1	24.0 (2)	100.1–107.1	103.9 (4)

RD = replacement dolomite; PC = pore-filling calcite; PD = pore-filling dolomite.

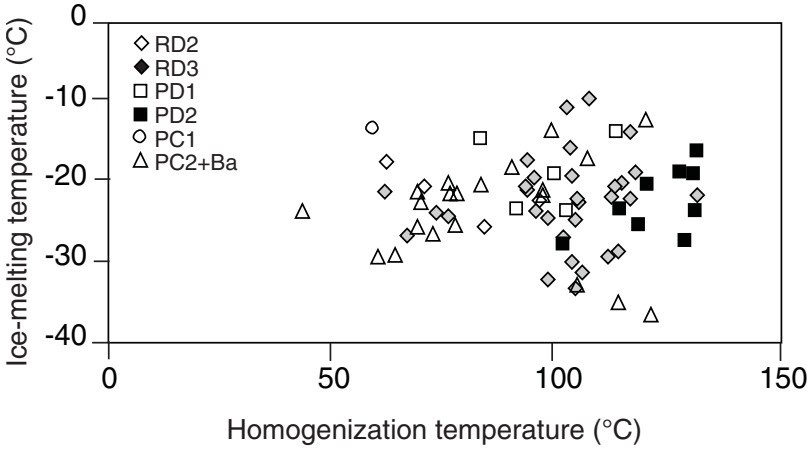

Figure 5.

Ice-melting temperature versus homogenization temperature diagram of fluid inclusions from the Romaine Formation. RD = replacement dolomite, PD = pore-filling dolomite, PC = pore-flling calcite, Ba = barite

STABLE ISOTOPES

Carbon and oxygen isotopes of carbonate

Various carbonate phases identified by petrography were sampled by a microdriller for C and O isotope study. Some phases are difficult to separate, and mixtures of known phases were sampled. A total of 39 samples were analyzed. The results are listed in Table 5 and illustrated in Figure 6.

Mixtures of sedimentary calcite and replacement calcite or early pore-filling calcite yield $\delta^{18}O$ (PDB) values from –6.8 ‰ to –6.0 ‰ and $\delta^{13}C$ (PDB) values from –3.0‰ to +0.2‰. These values largely fall in the ranges of Early to Middle Ordovician marine calcite (Qing and Veizer, 1994), consistent with the inference that they were formed in sedimentary or early diagenetic environments.

Mixtures of first- and second-phase replacement dolomite show similar $\delta^{18}O$ and $\delta^{13}C$ values as pure second-phase replacement dolomite. Except for one outlier at $\delta^{18}O$ –8.3‰ and $\delta^{13}C$ –1.6‰, $\delta^{18}O$ and $\delta^{13}C$ values of first- and second-phase replacement dolomite fall in the range from –6.2‰ to –2.0‰, and from –3.8‰ to +1.1‰, respectively. If the $\delta^{18}O$ values of the three earliest calcification events (–6.8 ‰ to –6.0‰) are taken to represent marine calcite values, and if a difference of 4‰ is assumed between calcite and dolomite (*see* Veizer, 1983, p. 274), then the $\delta^{18}O$ values of marine dolomite are expected to be from –2.8‰ to –2.0‰. Therefore, first- and second-phase replacement dolomite samples are slightly to moderately depleted in ^{18}O with respect to marine dolomite, which is consistent with the inference that they were formed during early diagenesis.

The $\delta^{18}O$ and $\delta^{13}C$ values of third- and fourth-phase replacement dolomite are similar, ranging from –7.6‰ to –5.0‰, and –1.5‰ to –0.1‰, respectively. Third- and fourth-phase replacement dolomite partly overlap with, and are generally more depleted in ^{18}O than first- and second-phase replacement dolomite, implying that the third and fourth phases were formed at higher temperatures. First- and second-phase pore-filling dolomite are further depleted in ^{18}O with respect to third- and fourth-phase replacement dolomite. Among the four samples analyzed, three form a tight cluster with $\delta^{18}O$ from –8.9‰ to –8.5‰ and $\delta^{13}C$ from –0.8‰ to –0.5‰, and one (first-phase pore-filling dolomite) lies at $\delta^{18}O$ –6.4‰ and $\delta^{13}C$ –2.7‰. The $\delta^{13}C$ values of most

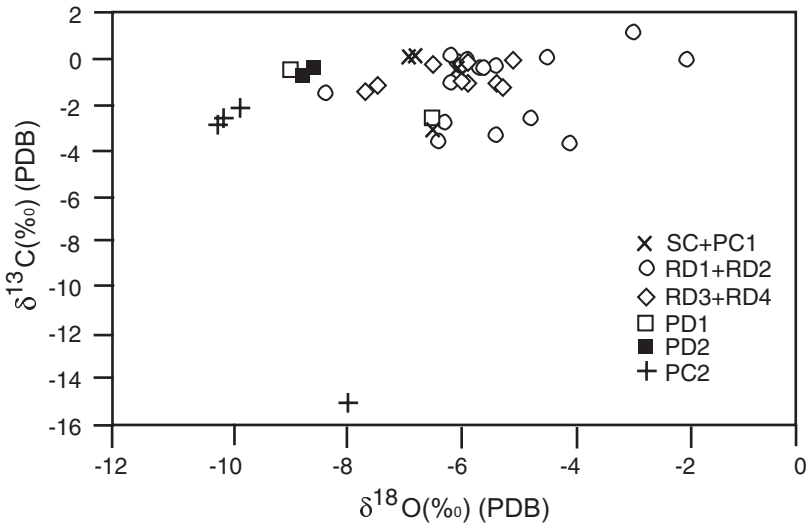

Figure 6.

$\delta^{13}C$ versus $\delta^{18}O$ diagram of carbonate phases from the Romaine Formation. SC = sedimentary calcite, PC = pore-filling calcite, RD = replacement dolomite, PD = pore-filling dolomite.

Table 5. Results of O and C isotope studies.

Sample#	Mineral(s)	$\delta^{18}O$ (‰) (PDB)	$\delta^{13}C$ (‰) (PDB)
NACP-13	RD1 (40%) + RD2 (60%)	-4.0	-3.8
NACP-24	RD1 (20%) + RD2 (80%)	-4.7	-2.7
NACP-24	RD1 (95%) + RD2 (5%)	-5.3	-3.4
NACP-38	RD2	-5.3	-0.4
NACP-39	RD4	-5.3	-1.1
NACP-39	RD2	-4.4	0.0
NACP-46	RD3	-5.8	-1.1
NACP-40	RD3	-5.9	-1.0
NACP-44	PC2	-10.1	-2.7
NACP-44	RD3	-5.0	-0.1
NACP-51	RD3	-5.2	-1.3
NACP-51	PC2	-10.2	-2.9
LGCP-33	SC (80%) + RC (20%)	-6.8	0.2
LGCP-33	SC (40%) + RC (60%)	-6.7	0.2
LGCP-4	RD2	-2.0	-0.1
LGCP-3	RD2	-6.2	-2.8
LGCP-3	PD1	-6.4	-2.7
LGCP-14	RD2	-8.3	-1.6
LGCP-14	RD3	-7.6	-1.5
LGCP-18	RD2	-6.0	-0.2
LGCP-18	RD3	-5.8	-0.2
LGCP-25	RD2	-5.6	-0.5
LGCP-25	PD1	-8.9	-0.6
LGCP-25	RD1	-5.9	-0.4
LGCP-26	RD2	-6.1	0.1
LGCP-26	RD4	-5.8	-0.2
LGCP-24	PD2	-8.5	-0.5
LGCP-24	RD2	-2.9	1.1
LGCP-28	RD2	-5.5	-0.5
LGCP-28	PC2	-9.8	-2.2
LGCP-31	SC (50%) + PC1 (50%)	-6.0	-0.3
LGCP-31	SC (90%) + RC (10%)	-6.4	-3.0
LGCP-31	PC2	-7.9	-15.1
LGPL-3	RD1 (40%) + RD2 (60%)	-6.3	-3.7
LGPL-10	RD2	-5.8	-0.1
LGPL-10	RD3	-6.4	-0.3
LGPL-10	PD2 (80%) + RD3 (20%)	-8.7	-0.8
QFT-1	RD2	-6.1	-1.1
QFT-1	RD3	-7.4	-1.2

RD = replacement dolomite; PC = pore-filling calcite; SC = sedimentary calcite; RC = replacement calcite; PD = pore-filling dolomite

dolomite phases fall within the range of limestone. A few first- and second-phase replacement dolomite samples are slightly depleted in ^{13}C with respect to limestone (Fig. 6).

Late pore-filling calcite is significantly depleted in ^{18}O with respect to sedimentary calcite and early pore-filling calcite. Among the four samples analyzed, three form a tight cluster with $\delta^{18}O$ from –10.2 ‰ to –9.8‰ and $\delta^{13}C$ from –2.9‰ to –2.2‰, and one lies at $\delta^{18}O$ –7.9‰ and $\delta^{13}C$ –15.1‰. The cluster is slightly depleted, and the outlier is strongly depleted in ^{13}C with respect to limestone (Fig. 6).

Sulphur isotopes of sulphides and sulphate

A few samples of sulphides (pyrite and sphalerite) and sulphate (barite) were analyzed for S isotopes. The results are shown in Table 6.

Table 6. Results of S isotope studies.

Sample#	Mineral	$\delta^{34}S$ (‰) (CDT)
NACP-51	Pyrite (Py3)	27.0
LGCP-31	Pyrite (Py3)	49.0
LGCP-28	Pyrite (Py3)	44.6
NACP-51	Barite	35.2
NACP-35	Sphalerite	4.7

One barite and three pyrite (Py3) samples show very high $\delta^{34}S$ values, ranging from +27.0‰ to +49.0‰. These values are higher than modern seawater (around +20‰) and marine evaporite deposits (+22‰) (Ohmoto and Goldhaber, 1997), or Early to Middle Ordovician marine evaporite deposits (about +25‰ to +30‰, Ohmoto and Rye, 1979). The sphalerite sample gives a $\delta^{34}S$ value of +4.7‰, which is significantly lower than marine sulphates.

DISCUSSION AND CONCLUSIONS

By comparing porous and nonporous dolostone samples (Table 7), it is noticed that porous dolostone contains at least one of the following dolomite phase: third- or fourth-phase replacement dolomite, or first- or second-phase pore-filling dolomite, whereas nonporous dolostone comprises predominantly first- and second-phase replacement dolomite, with or without first- and second-phase pore-filling dolomite. Porosities are related to third- and fourth-phase replacement and first- and second-phase pore-filling dolomite in two ways: 1) intercrystal porosities were created by third- and fourth-phase replacement dolomite, and 2) porosities were created by dissolution of first- and second-phase replacement dolomite by fluids associated with the formation of third- and fourth-phase replacement and first- and second-phase pore-filling dolomite. From the observation that late-stage sulphide (Py3) and sulphate (barite) are significantly enriched in ^{34}S relative to marine evaporite, it is inferred that significant amounts of sulphides with low $\delta^{34}S$ values (e.g. sphalerite) could have been precipitated at an earlier stage, producing acid fluids causing the dissolution of carbonate.

Since porosities are closely related to third- and fourth-phase replacement and first- and second-phase pore-filling dolomite, it is worthwhile to further discuss the nature of the fluids associated with these dolomite phases. Both fluid-inclusion and C-O isotope data clearly indicate that third- and fourth-phase replacement and first- and second-phase pore-filling dolomite were formed from warm basinal brines; however, it is not straightforward if these fluids were normal burial diagenetic fluids or hydrothermal fluids advected from deeper parts of the basin. According to Bertrand (1990), the maximum burial temperatures (based on organic matter reflectance data) of the Romaine Formation in the LGPL, NACP, and LGCP wells are about 147°C, 133°C, and 115°C, respectively. The maximum homogenization temperatures of fluid inclusions from the LGPL, NACP, and LGCP wells are 137.1°C (second-phase pore-filling dolomite), 131.4°C (second-phase pore-filling dolomite), and 131.3°C (third-phase replacement dolomite), respectively. Because pressure corrections for the homogenization temperatures are likely to be fairly small, it seems that the dolomitization could have taken place at maximum burial from the point of view of thermal constraint. This kind of

Table 7. Comparison of carbonate phases (%) between porous and nonporous dolostone. Darkened boxes highlight the occurrence of third- and fourth-phase dolomite and first- and second-phase pore-filling dolomite.

Sample#	RD1	RD2	RD3	RD4	PD1	PD2	RC	PC2	Porosity
Nonporous dolostone									
NACP-13	40	57							0%
NACP-24	78	20						1	0%
NACP-35	80	15						2	0%
LGCP-4	7	90						1	0%
LGCP-3		60			25		10	15	0%
LGPL-3	40	55				5			0%
Porous dolostone									
NACP-40	9		80		1			10	10%
NACP-54	60	20			10			9	1%
NACP-38		82			5			10	15%
NACP-39		85	12	2				1	10%
NACP-46			99						15%
NACP-44			85					14	2%
NACP-51		15	83			2			5%
NACP-37	25	45				5		5	2%
LGCP-14		70	30						10%
LGCP-18		24	75						20%
LGCP-25	50	45			5				5%
LGCP-26		35		65					10%
LGCP-24		73	10			10		2	10%
LGCP-28	20	75				2		2	3%
LGPL-10		30	53			10		2	7%
QFT-1		80	20						7%

RD = replacement dolomite; PD = pore-filling dolomite; RC = replacement calcite;
PC = pore-filling calcite

relationship between fluid-inclusion homogenization temperatures and thermal maturity of organic matter in host rocks is not unusual. In fact, most Mississippi Valley-type lead-zinc deposits or districts show this kind of thermal relationship, e.g. Pine Point, Newfoundland Zinc, East Tennessee, Central Missouri, Northern Arkansas, and Tri-State (Sangster et al., 1994); yet for all these Mississippi Valley-type deposits mineralization and associated dolomitization are thought be related to hydrothermal fluids derived from deeper parts of associated basins. A comparison with the data from Newfoundland Zinc (Lane, 1990) indicates that the diagenetic characteristics of the dolostone beds of the Romaine Formation are similar to those in the St. George Group in western Newfoundland, where dolomitization and Zn mineralization as well as oil reservoir formation (Cooper at al., 1997) are related to hydrothermal fluids. Given the similarity in stratigraphic position and geological setting between western Newfoundland and Anticosti Island, we tentatively interpreted that the late dolomitization (third-phase replacement dolomite–fourth-phase replacement dolomite–first-phase pore-filling dolomite–second-phase pore-filling dolomite) in the Romaine Formation was caused by hydrothermal fluids derived from deeper parts of the basin.

In conclusion, petrographic, fluid-inclusion, and stable isotope data indicate that there are several types of dolomite in the Romaine Formation, ranging from early diagenesis to late hydrothermal alteration. Early diagenetic dolomitization (first- and second-phase replacement dolomite) did not create porosity. Significant porosities were produced by dissolution and further dolomitization (third- and fourth-phase replacement dolomite), which is thought to be related to hydrothermal fluids derived from deeper parts of the basin. The occurrence of oil inclusions in late calcite cement and barite indicates a petroleum migration event after the formation of dissolution- and dolomitization-related porosity.

ACKNOWLEDGMENTS

We thank Rudolf Bertrand for providing the sample from the QFT quarry north of Mingan Islands and for reviewing the manuscript. Financial support from Shell Canada is gratefully acknowledged.

REFERENCES

Bertrand, R.
1990: Maturation thermique et histoire de l'enfouissement et de la génération des hydrocarbures du bassin de l'archipel de Mingan et de l'Île d'Anticosti; Canadian Journal of Earth Sciences, v. 27, p. 731–741.
1991: Maturation thermique des roches mères dans les bassins des basses-terres du Saint-Laurent et dans quelques buttes témoins au sud-est du Bouclier canadien; International Journal of Coal Geology, v. 19, p. 359–383.

Cooper, M., Weissenberger, J., Hostad, D., Gillespie, D., Rae, D., Clark, E., and Knight, I.
1997: Exploring for giant oil fields in the Cambro-Ordovician of western Newfoundland; the story so far; Canadian Society of Petroleum Geologists, Reservoir, v. 24, p. 6.

Desrochers, A.
1985: The Lower and Middle Ordovician platform carbonates of the Mingan Islands, Quebec: Stratigraphy, sedimentalogy, paleokarst, and limestone diagenesis; Ph.D. thesis, Memorial University of Newfoundland, St. John's, Newfoundland, 454 p.

Desrochers, A. and James, N.P.
1988: Early Paleozoic surface and subsurface paleokarst: Middle Ordovician Carbonates, Mingan Islands, Quebec; *in* Paleokarst, (ed.) N.P. James and P.W. Choquette; Springer-Verlag, New York, New York, p. 183–210.

Goldstein, R.H. and Reynolds, T.J.
1994: Systematics of fluid inclusions in diagenetic minerals; Society of Economic Paleontologists and Mineralogists, Short Course 31, 199 p.

Kesler, S.E.
1994: Mississippi Valley-type deposits in continental margin basins: lessons from the Appalachian-Caledonian orogen; *in* Sediment-hosted Zn-Pb Ores, (ed.) L. Fotebote and M. Boni, Springer-Verlag, Berlin Heidelberg, p. 89–103.

Knight, I., James, N.P., and Lane, T.E.
1991: The Ordovician St. George Unconformity, northern Appalachians: the relationship of plate convergence at the St. Lawrence Promontory to the Sauk-Tippecanoe sequence boundary; Geological Society of America, Bulletin, v. 103, p. 1200–1225.

Lane, T.E.
1990: Dolomitization, brecciation and zinc mineralization and their paragenetic, stratigraphic and structural relationships in the Upper St. George Group (Ordovician) at Daniel's Habour, western Newfoundland; Ph.D. thesis, Memorial University of Newfoundland, St. John's, Newfoundland, 565 p.

Ohmoto, H. and Goldhaber, M.B.
1997: Sulfur and Carbon Isotopes; *in* Geochemistry of Hydrothermal Ore Deposits, (ed.) H.L. Barnes; John Wiley & Sons, New York, New York, p. 517–611 (third edition).

Ohmoto, H. and Rye, R.O.
1979: Isotopes of Sulfur and Carbon; *in* Geochemistry of Hydrothermal Ore Deposits, (ed.) H.L. Barnes; John Wiley & Sons, New York, New York, p. 509–567 (second edition).

Qing, H. and Veizer, J.
1994: Oxygen and carbon isotopic composition of Ordovician brachiopods: implications for coeval seawater; Geochimica et Cosmochimica Acta, v. 58, p. 4429–4442.

Roedder, E.
1984: Fluid inclusions; Reviews in Mineralogy, v. 12, 644 p.

Sanford, B.V.
1993: St. Lawrence Platform – Geology; Chapter 11 *in* Sedimentary Cover of the Craton in Canada, (ed.) D.F. Stott and J.D. Aitken; Geological Survey of Canada, Geology of Canada, no. 5, p. 723-786 (*also* Geological Society of America, The Geology of North America, D-1).

Sangster, D.F., Nowlan, G.S., and McCracken, A.D.
1994: Thermal comparison of Mississippi Valley-Type lead-zinc deposits and their host rocks using fluid inclusion and conodont color alteration index data; Economic Geology, v. 89, p. 493–514.

Saunders, C., Strong, D.F., and Sangster, D.F.
1992: Carbonate-hosted lead-zinc deposits of western Newfoundland; Geological Survey of Canada, Bulletin 419, 78 p.

Veizer, J.
1983: Trace elements and isotopes in sedimentary carbonates; Reviews in Mineralogy, v. 11, p. 265–299.

Geological Survey of Canada Project 990001AG